inter·noise 2011

Osaka Japan September 4-7

Slat Noise Simulations: Status and Challenges

Meelan Choudhari[1], David Lockard[2], Mehdi Khorrami[3], and Raymond Mineck[4]

[1,2,3] NASA Langley Research Center, M.S. 128, Hampton, VA 23681

[4] Vigyan, Inc., Hampton, VA 23666

ABSTRACT

Noise radiation from the leading edge slat of a high-lift system is known to be an important component of aircraft noise during approach. NASA's Langley Research Center is engaged in a coordinated series of investigations combining high-fidelity numerical simulations and detailed wind tunnel measurements of a generic, unswept, 3-element, high-lift configuration. The goal of this effort is to provide a validated predictive capability that would enable identification of the dominant noise source mechanisms and, ultimately, help develop physics inspired concepts for reducing the far-field acoustic intensity. This paper provides a brief overview of the current status of the computational effort and describes new findings pertaining to the effects of the angle of attack on the aeroacoustics of the slat cove region. Finally, the interplay of the simulation campaign with the concurrently evolving development of a benchmark dataset for an international workshop on airframe noise is outlined.

Keywords: Airframe Noise, Leading Edge Slat, High-Lift Noise

1. INTRODUCTION

With the advent of quieter, ultra-high-bypass-ratio engines, flow unsteadiness in the vicinity of various airframe components has emerged as an important contributor to the noise signature of subsonic commercial transports during their approach for landing. Both model-scale tests and flyover noise measurements have shown that the leading-edge slat can be a prominent source of airframe noise during approach conditions. Depending on the size of the aircraft, at full scale, the maximum slat noise levels typically occur between 100 Hz and 400 Hz.

Slat noise is primarily broadband, but may be accompanied by multiple narrowband, tonal peaks that also occur within the frequency range of the highest broadband noise. The occurrence of the tones may be configuration dependent. Measurements by Pott-Pollenske et al. [1] suggest that the tonal peaks appear above a certain angle of attack (AOA) and become stronger as the AOA is increased across the typical range for aircraft approach for landing. For realistic high-lift configurations with non-zero sweep and taper, the tones are significantly weaker (and more easily controllable via boundary layer tripping just upstream of the slat cusp) in comparison with simplified configurations without 3-D effects. Subscale tests indicate that the tonal frequencies scale as Strouhal numbers based on the free-stream speed and not with any local velocities near the slat cove region. The tonal frequencies do not correspond to a harmonic sequence; they vary with the angle of attack, but no clear trend has been delineated on the basis of existing data. It was speculated in [1] that the tones may arise from low-frequency oscillations of the slat cove region, along with possible coupling with geometric or aerodynamic resonance effects.

Computational simulations have become an increasingly valuable tool in airframe noise research. Simulations can serve as a high-fidelity prediction tool to minimize expensive testing and guide model development, contribute to the understanding of the noise generation mechanisms, as well as to evaluate candidate noise reduction concepts. Simulations of the noise due to high-lift devices are

---

[1] Meelan.M.Choudhari@nasa.gov
[2] David.P.Lockard@nasa.gov
[3] Mehdi.R.Khorrami@nasa.gov
[4] Raymond.E.Mineck@nasa.gov

deemed particularly useful because of the difficulties in performing meaningful measurements because of the sensitivity to flow Reynolds number (i.e., scaling effects), large-scale 3-D effects even when the geometry is nominally 2D, a lack of convenient and non-intrusive access to the flow features to be measured, and increased challenges in measuring both aerodynamic and acoustic fields in the same facility.
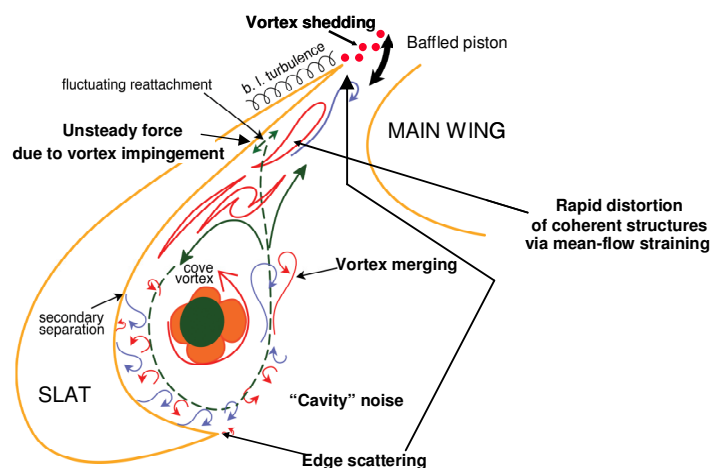

Figure 1 – Potential sources and physical mechanisms behind noise generation near a leading edge slat [2]

Slat noise is a complex aeroacoustic problem consisting of several different physical mechanisms (Fig. 1). To provide a fundamental understanding of the slat noise sources and develop a validated prediction capability, NASA Langley has been engaged in a series of synergistic wind tunnel and computational investigations of a generic, unswept, 3-element, high-lift configuration. This so called 30P30N configuration, designed by McDonnell-Douglas (now Boeing), has been used for various measurements of the unsteady flow near the slat in NASA's Basic Aerodynamic Research Tunnel (BART) [3]. Accompanying numerical simulations have addressed the details of the unsteady flow structures [2, 4], provided comparisons with BART measurements [2], evaluated noise prediction [5], and examined the effects of sweep [6] as well as flow Mach number, and Reynolds number [7] in limited parameter studies. These references also describe other pertinent work in the literature, which is mostly excluded from this paper due to space limitations.

The above computational studies provide the foundation for assessing the current state of the art in computational predictions of slat cove aeroacoustics. Because detailed comparisons of the computed near-field unsteady flow with the BART measurements have already been presented in [2], we emphasize the acoustic features in this paper with a focus on extending the previous results to include the effects of model angle of attack and making comparisons with an empirical model for slat noise [8].

2. EFFECT OF ANGLE OF ATTACK ON SLAT COVE AEROACOUSTICS

The 30P30N model tested in the BART at NASA Langley Research Center represents a generic, 3-element, zero-sweep, high-lift configuration with slat and flap deflections of 30° each. The slat chord and flap chord of the model are equal to 15 and 30 percent, respectively, of the stowed chord of 0.457 m. At the test Mach number of $M = 0.17$, the Reynolds number, based on the stowed chord of the BART model, corresponds to 1.7 million. To focus on the slat broadband noise in the computations, the (small but nonzero) trailing-edge thickness is artificially sharpened to zero. To enable acoustic predictions without involving reflections from tunnel walls, computations are performed in free-flight mode for AOA equal to 3, 5.5, and 8.5 deg. Near-field computations with a quasi-laminar slat cove region and Menter's SST model were combined with acoustic propagation using Ffowcs Williams−Hawkings (FWH) form of acoustic analogy. The spanwise extent of the computational domain corresponds to 0.75 c_s, where c_s denotes the slat chord. For details of the rigging parameters, the computational procedure, and the spatial grid, the reader is deferred to Refs. [2, 5].

2.1   Surface Pressure Distribution

The mean pressure distribution along the model surface (Figs. 2(a)-(b)) provides a useful starting point for understanding the effects of AOA on slat cove aeroacoustics. With increasing AOA, the stagnation point moves progressively closer to the slat cusp.   This has the effect of shortening the region of flow acceleration ahead of the boundary layer separation from the slat surface, resulting in a larger Cp at the cusp location for higher AOA.   A similar trend is observed in the pressure peak along the slat cove surface where the slat cove flow reattaches just ahead of the trailing edge (Fig. 2(b)).   On the other hand, because of the increased flow acceleration along the upper surface at higher AOA, the flow velocity near the slat trailing edge increases correspondingly, which in turn amounts to a stronger flow acceleration between the reattachment location and the slat trailing edge (Fig. 2(b)).   These trends in the mean flow behavior have an impact on the strength and the evolution of unsteady flow structures within the slat cove region.

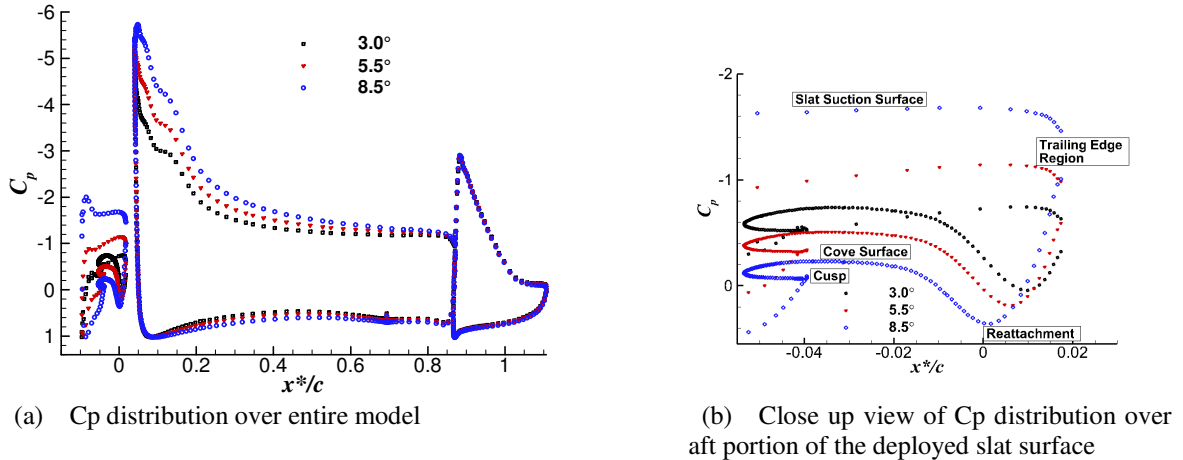| (a)   Cp distribution over entire model | (b)   Close up view of Cp distribution over aft portion of the deployed slat surface |

Figure 2. Effect of AOA on mean surface pressure distribution

2.2   Near-Field Unsteady Flow

The distribution of root-mean-square (r.m.s.) pressure fluctuation along the model surface is shown in Fig. 3. As discussed previously in [2], the highest pressure fluctuations occur near the reattachment location.   A weaker peak in pressure fluctuation occurs along the main wing's leading edge, which is exposed to the gap between the slat and the main wing.   However, this latter peak is lower in comparison with the peak along the slat surface by approximately 8dB at 3 deg AOA and by 11 dB at 8 deg AOA.   There is an additional peak near the main element cove; however, because of its highly localizednature, it does not contribute significantly to the radiated noise.

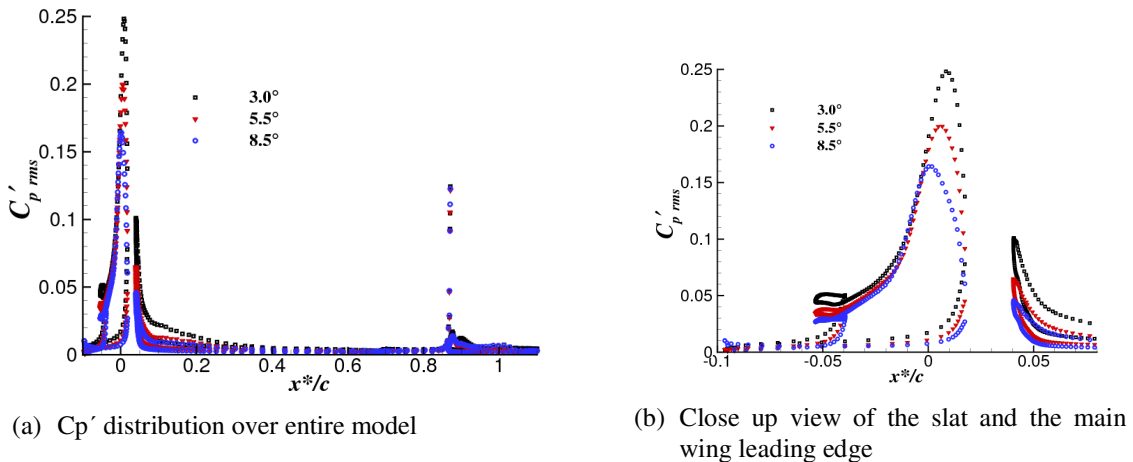| (a) Cp′ distribution over entire model | (b) Close up view of the slat and the main wing leading edge |

Figure 3. Effect of AOA on r.m.s. surface pressure distribution

The distribution of turbulence kinetic energy (TKE) based on the resolved fluctuations within the slat cove region (Figs. 4(a)-(c)) indicates the mean trajectory of the shear layer surrounding the recirculating flow region in the slat cove. The computed TKE levels generally compare well with those measured in the wind tunnel [2]. As discussed in [2], the highest levels of TKE occur near the reattachment location as the unsteady structures within the shear layer approach the slat surface and, subsequently, either accelerate towards the trailing edge or get convected back towards the slat cusp. The TKE distribution exhibits two local maxima within the reattachment region, one of which lies just ahead of the reattachment location and the other, typically higher maximum occurs along a narrow ridge within the contours as seen most clearly in Fig. 4(b). A third (and weaker) maximum is also observed within the slat shear layer. The qualitative distribution of TKE is similar for all three AOA, but the TKE levels near all three peaks decrease at higher AOA. This trend is consistent with the decreasing shear across the slat mixing layer, corresponding to the progressively weaker acceleration ahead of flow separation near the cusp as described earlier in the context of Fig. 2. The variations in TKE levels at all three peaks correlate quite well with the corresponding variation in the peak r.m.s. surface pressure fluctuation and, not unexpectedly, the TKE peak just ahead of the reattachment location does the best job at mimicking the variation in the peak r.m.s. fluctuation in Cp.

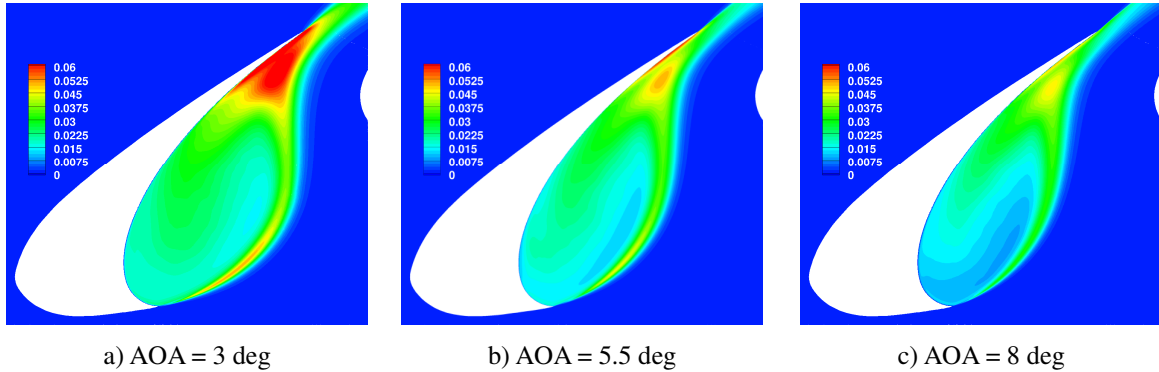a) AOA = 3 deg   b) AOA = 5.5 deg   c) AOA = 8 deg

Figure 4: Turbulence kinetic energy distribution within slat cove region

The frequency spectra of pressure fluctuations along the solid surface and velocity fluctuations at selected location within the slat shear layer were investigated (Fig. 5(a)). The autospectra of both the near-field pressure fluctuations near the slat trailing edge (Fig. 5(b)) and the vertical velocity fluctuations within the slat shear layer (Figs. 5(c)-(d)) display weak evidence of narrowband peaks that appear to become more prominent with an increase in the AOA. This behavior is consistent with the measured trend in the far-field acoustic spectrum from wind tunnel experiments by DLR researchers [1]. Similar narrow-band peaks have been observed in the near-field spectra obtained using a different simulation code [9, 10]. Interestingly, the frequencies corresponding to the first few dominant peaks from the autospectra in [10] are close to the current predictions; however, the magnitude of the peaks was considerably higher in those results.

2.3   Acoustic Characteristics

In comparison with the frequency spectra at probe locations within the acoustic source region, the tonal peaks are much more prominent within the auto-spectra corresponding to probe locations that fall outside of the slat cove region (Figs. 6(a)-(c)). However, unlike the DLR measurements [1], the tonal behavior at the latter probe locations appears to be almost equally strong at all three AOA.

The intensification of narrow-band peaks within the acoustic spectra (whether they correspond to probe locations in the vicinity of the source region (Figs. 6(a)-(b)) or in the acoustic far field (Fig. 6(c)) may suggest an acoustic origin for the resonances associated with these peaks. On the other hand, the computational results from [7] for varying flow Mach number are suggestive of a Strouhal number scaling for the peak frequencies. Furthermore, the tonal peaks in the near-field spectra (Fig. 5) become highly prominent when the spanwise coherence length is plotted as a function of frequency, indicating significantly increased correlation lengths at the tonal frequencies. In [5], the coherence

length was shown to increase by a factor of as much as two or more for the Strouhal numbers that fall within the frequency band of peak pressure fluctuations (1< St < 3, where the Strouhal number St is based on the slat chord and free-stream velocity).
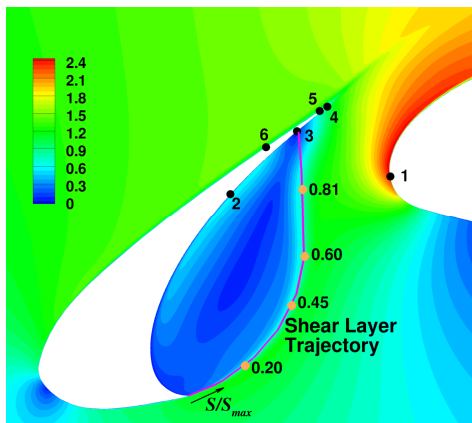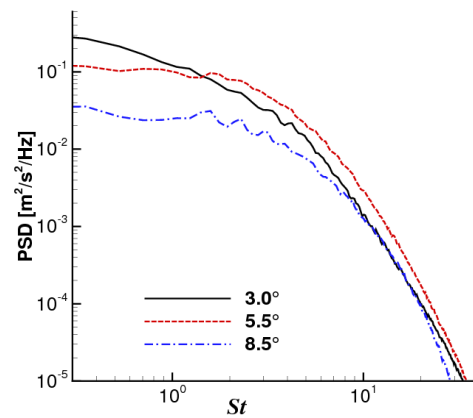

a) Magnitude of mean planar velocity near slat for 5.5 deg AOA. The figure also illustrates the probe locations investigated in detail (S is the distance along the shear layer trajectory) [7]
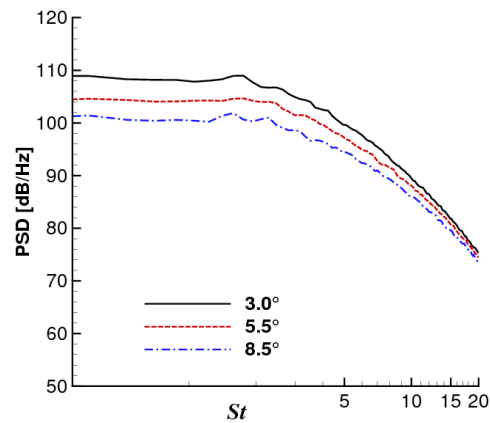
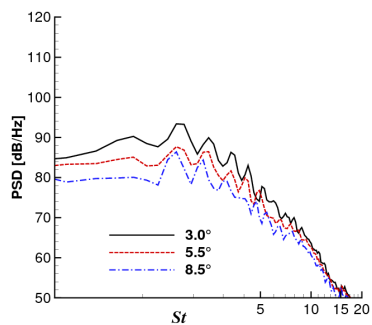b) Autospectra of p´ near trailing edge (point 4 in part (a) of the figure)
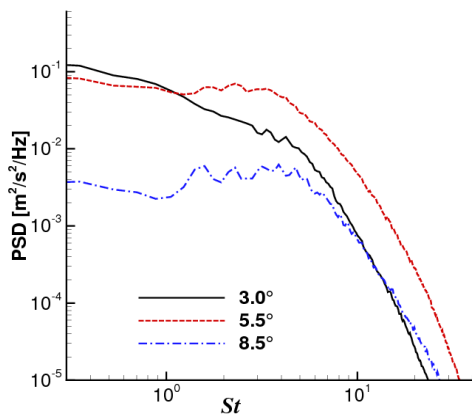
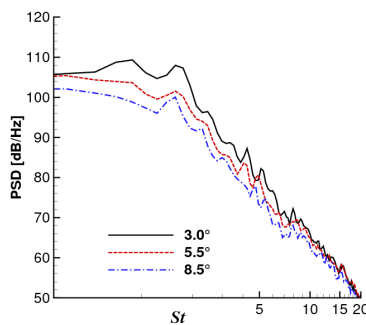c) v´ autospectra at 60% of the shear layer trajectory from slat cusp to reattachment location

d) v´ autospectra at 81% of the shear layer trajectory from slat cusp to reattachment location

Figure 5: Autospectra of source region fluctuations
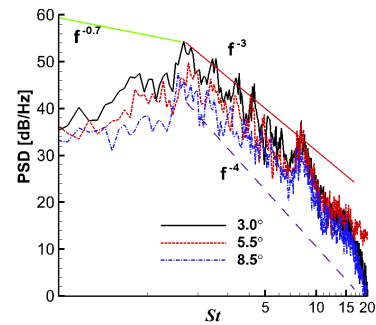
Figure 5: Autospectra of source region fluctuations

a) Slat upper surface (point 6 from Fig. 5(a))

b) Wing leading edge (point 1 from Fig 5(a))

c) Far-field acoustics at 10 chord lengths below the model

Figure 6: Auto-spectra of p' at selected points outside the source region

In general, the levels of the acoustic spectra decrease with an increase in AOA, a trend that was noted during the earlier computations in [9]. The high-frequency roll-off in far-field acoustic spectra (Fig. 6(c)) appears similar to the $f^{-2.8}$ decay according to the empirical model in [8], but a more definitive agreement cannot be established because of insufficient averaging (and finite Fourier bin width) resulting from limited temporal duration of the numerical data. At low frequencies, the power spectral density (PSD) in Fig. 6(c) increases with the Strouhal number, whereas the empirical model from [8] would have predicted a weak decay ($\sim f^{-0.7}$) in the PSD. It should be noted that Ewert et al. [11] were able to mimic the measured $f^{-0.7}$ decay from an experiment with a different high-lift configuration. Furthermore, even though the underlying methodology for acoustic predictions was rather different from the more direct method used herein, the acoustic predictions (not shown) from [11] for the 30P30N model matched very well with the current results for 5.5 deg AOA. Since the same code predicted different low-frequency behaviors for the two different high-lift configurations, the question arises as to whether the low-frequency behavior of far-field acoustic spectra is highly configuration dependent. Clearly, detailed time-accurate measurements for the present 30P30N configuration would go a long way to help settle this question.

The in-plane directivity of the overall sound pressure level (OASPL) was computed using the Ffowcs Williams–Hawkings (FWH) form of acoustic analogy in conjunction with the surface pressure fluctuations from the CFD solutions. The results are shown in Fig. 7(a), which also includes the directivity pattern for 5.5 deg AOA based on a computational domain with a longer spanwise length of 2.26 slat chords, i.e., three times the spanwise extent of the present domain [5]. Note that using the fluctuation data along the solid surface does not account for either the quadrupole noise sources within the flow or the effects of non-uniform mean flow in the vicinity of the model. However, previous computations [7] involving an off-body, permeable FWH surface have shown the neglected effects to be small, and primarily confined to the rear arc region between θ=300 deg to θ=45 deg, where θ is measured relative to the flow direction and θ=270 deg corresponds to the overhead direction.

Each of the directivity patterns in Fig. 7(a) are marked by two prominent minima, one of them being close to the 230 deg meridian and the other one being closely aligned with the downstream direction. The orientations of these two minima are approximately consistent with the presence of baffle surfaces along the slat chord and the main wing, respectively. Indeed, the shifts in both minima as well as in the maximum of the upper lobe in going from 3 deg AOA to 5.5 deg AOA are very nearly equal to the corresponding increment in AOA between the two cases. Analogous shifts in the directivity pattern from 5.5 deg AOA to the 8.5 deg AOA case are also qualitatively consistent with the above trend between 3 deg and 5.5 deg AOA cases, but the numerical differences between the two higher-AOA cases deviate significantly from the 2.5 deg AOA increment between them. The reasons behind this discrepancy are the target of continuing investigation.

As seen from Fig. 7(a), the upper portion of the directivity pattern does not involve any secondary lobes in the vicinity of the peak direction, but the lower portion does involve dual peaks bracketing the overhead direction. An additional, rather flat peak is observed within the rear arc quadrant, along an orientation that is approximately normal to the slat chord. The multiple lobes in the lower half directivity indicate the potential influence of reflections from the different components of the high-lift configuration. The shift with AOA in the angular orientation of the peak directivity location near θ=290 deg is found to be close to the corresponding increments in the AOA parameter.

The increment in the rear arc peak near θ = 290 deg corresponding to a decrease in AOA from 8.5 to 5.5 deg is approximately 3.4 dB, whereas the corresponding increment when the AOA is reduced from 5.5 deg to 3 deg is nearly 4 dB. These changes indicate a faster than linear scaling in the OASPL with respect to the maximum of the mean square fluctuation in surface pressure coefficient near the reattachment location of the slat cove shear layer (Fig. 3). In fact, the variation is very nearly quadratic. The faster than linear variation indicates that approximately one half of the increment in OASPL with a decreasing angle of attack must be accounted for by an increased efficiency in converting the hydrodynamic source into acoustic fluctuations. Qualitatively, at least, the increased

efficiency may arise from the movement of the reattachment location towards the trailing edge. However, the as yet unknown physics associated with the narrowband tones may contribute to the above trend in OASPL as well.   For AOA = 5.5 deg, the acoustic intensity per unit span based on the longer spanwise domain (z_{max} = 2.26 c_s) of Ref. [5] is significantly larger than that obtained with the shorter domain used in present computations, despite the fact that the spanwise correlation drops to near zero values even within the present domain. This may be due to a substantially higher spanwise coherence of the near-field unsteadiness for frequencies corresponding to the narrowband spectral peaks.

(a)   Overall SPL

(b) Narrow-band directivity at selected frequencies for 5.5 deg AOA
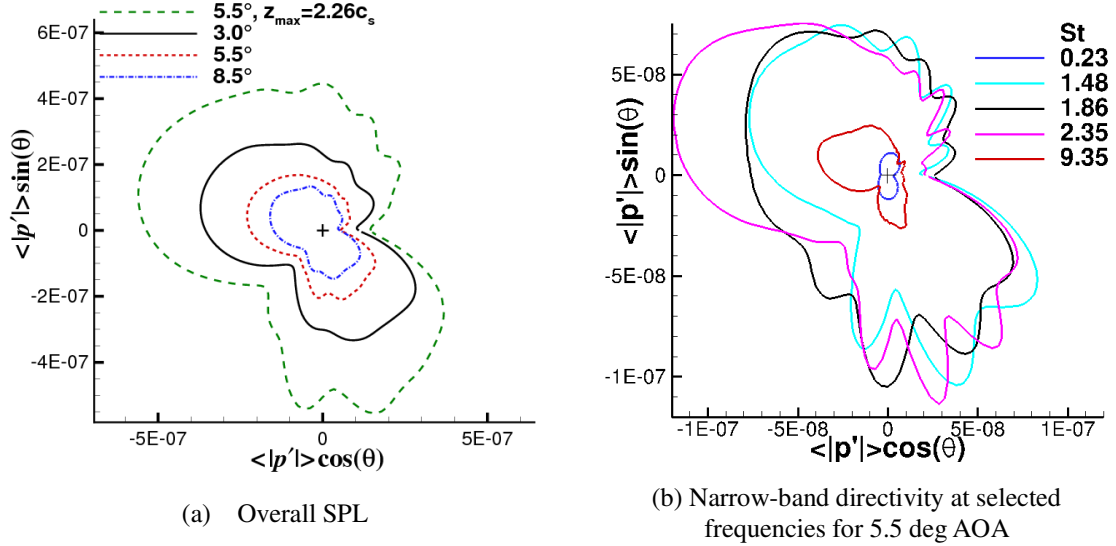
Figure 7. Effect of AOA on acoustic directivity at 10 chord lengths from the slat trailing edge.   The unsteady pressure is normalized by ρa^2 where ρ denotes the free-stream density and a represents the speed of sound.

Narrow band directivities summed over 1/3rd octave bands centered on selected values of acoustic frequency are indicated in Fig. 7(b).   The directivity pattern at the lowest frequency (St = 0.23), for which the chord length of the entire high-lift configuration is smaller than the acoustic wavelength, resembles the directivity for a simple dipole.   At each of the intermediate frequencies (St = 1.48, 1.86, 2.35) that contribute a significant portion of the overall noise, the directivity within the lower half plane includes multiple lobes.   The smoother directivity of the overall SPL (Fig. 7(a)) is caused by the staggered peaks in adjacent frequency bands. At these frequencies, the combined chord length of the main wing and the flap is larger than the acoustic wavelength, which explains why the upper portion of the directivity pattern resembles the directivity pattern for edge scattering. The 1/3rd octave band directivity pattern centered on the highest frequency (St = 9.35) shows relatively weak radiation within the rear half plane.   Because of averaging over a larger number of bins, this pattern does not display the prominent lobes seen at the intermediate frequencies. .

3. FINAL REMARKS

This paper provided a brief overview of the ongoing computational effort related to the aeroacoustics of the generic, unswept 3-element, 30P30N high-lift configuration, with an emphasis on the effects of angle of attack between 3−8.5 degrees, i.e., the typical AOA range for aircraft landing approach.   The characteristics of both near-field unsteadiness within the slat cove region and the far-field acoustics were found to remain unchanged with the variations in AOA.   Mainly, an increased AOA results in reduced intensity of broadband slat noise, along with a rotation of the directivity pattern corresponding to the change in AOA.   To aid in the development of reduced order models and physics based correlations for slat noise, the far-field acoustic characteristics were related to more readily available flow parameters related to model geometry and the mean flow field.   Variations with AOA underscore the dominant role of near-field fluctuations near the reattachment location as the primary source of

noise.

For the most part, the simulation data supports the parametric dependence indicated by the DLR model, in addition to providing more detailed insights into the physical origin of that dependence. Despite the encouraging progress, a lot remains to be done for both a more definitive validation of the aeroacoustic computations and to understand the precise physical mechanisms underlying the conversion of slat cove unsteadiness into noise. This cannot be easily accomplished without a concerted effort by the airframe noise community that is focused on specific configurations of common interest. The series of workshops on Benchmark Problems for Airframe Noise Computations (BANC) reflects a grass-roots effort to accomplish this goal, and it is anticipated that the 30P30N configuration outlined in this paper will be included in the BANC-II workshop that will be held in June 2012 [12]. In that case, at least some of the questions raised in this paper should be resolved from the BANC-II studies.

ACKNOWLEDGEMENTS

REFERENCES

[1] M. Pott-Pollenske, J. Alvarez-Gonzalez, and W. Dobrzynski, "Effect of Slat Gap on Farfield Radiated Noise and Correlation with Local Flow Characteristics," AIAA Paper 2003-3228, 2003.

[2] M.M. Choudhari and M.R. Khorrami, "Effect of Three-Dimensional Shear-Layer Structures on Slat Cove Unsteadiness," AIAA Journal, Vol. 45, No. 9, 2007, pp. 2174–2186.

[3] L.N. Jenkins, M.R. Khorrami, and M. Choudhari, "Characterization of Unsteady Flow Structures Near Leading-Edge Slat: Part I. PIV Measurements," AIAA Paper 2004-2801, 2004.

[4] M.R. Khorrami, M. Choudhari, and L.N. Jenkins, "Characterization of Unsteady Flow Structures Near Leading-Edge Slat: Part II. 2D Computations," AIAA Paper 2004-2802, 2004.

[5] D.P. Lockard and M. Choudhari, "Noise Radiation from a Leading-Edge Slat," AIAA Paper 2009-3101, 2009.

[6] D.P. Lockard and M. Choudhari, "The Effect of Cross Flow on Slat Noise," AIAA Paper 2009-3835, 2010.

[7] D.P. Lockard and M. Choudhari, "Variation of Slat Noise with Mach and Reynolds Numbers," To be presented at the 17th AIAA/CEAS Aeroacoustics Conference, Portland, OR, June 6-8, 2011.

[8] M. Pott-Pollenske, W. Dobrzynski, H. Buchholz, B. Gehlhar, and F. Walle, "Validation of Semi-empirical Airframe Noise Prediction Method through Dedicated A319 Flyover Noise Measurements," AIAA Paper 2000-2470, 2000.

[9] R. Satti, Y. Li, R. Shock, and S. Noelting, "Computational Aeroacoustics Analysis of a High-Lift Configuration," AIAA Paper 2008-34, 2008.

[10] R.E. Mineck, "Application of Powerflow to the 30P30N High Lift Configuration," Final report, Task NNL08AM06T, NASA Langley Research Center, Jan. 2011.

[11] R. Ewert, J. Dierke, B. Muhlbauer, A. Neifeld, C. Appel, M. Sierfert, and O. Kornow, "CAA Broadband Noise Prediction for Aeroacoustic Design," Trilateral Seminar, 21-26 Sept. 2010. Svetiogorsk, Russia, 2010.

[12] https://info.aiaa.org/tac/ASG/FDTC/DG/BECAN_files_/BANCII.htm